Considerations for a high-performance thermionic energy conversion device based on a negative electron affinity emitter

Joshua Ryan Smith*
Department of Physics, North Carolina State University, Raleigh, North Carolina 27695-8202, USA

Griff L. Bilbro
Department of Electrical and Computer Engineering, North Carolina State University, Raleigh, North Carolina 27695-7911, USA

Robert J. Nemanich
Department of Physics, Arizona State University, Tempe, Arizona 85287-1504, USA

(Received 5 April 2007; revised manuscript received 17 October 2007; published 27 December 2007)

A theory is developed to model the effect a negative electron affinity (NEA) emitter electrode has on the negative space charge effect of a vacuum thermionic energy conversion device (TEC). The theory is derived by treating the electrons in the interelectrode space as a collisionless gas and self-consistently solving the Boltzmann transport equation and Poisson equation. The theory determines the point on the voltage-current characteristic such that the maximum motive due to space charge is at the same level as the conduction band minimum. It is shown that emitter electrodes with an NEA significantly mitigate the negative space charge effect; therefore a TEC employing such an electrode will outperfrom a similar TEC with conventional electrodes in terms of output power. Additionally, it is shown that a TEC with an NEA emitter electrode can have a greater interelectrode spacing than a TEC with conventional electrodes operating under similar conditions where the outputs of both TEC's are comparable.

DOI: 10.1103/PhysRevB.76.245327 PACS number(s): 81.05.Uw, 84.60.Ny, 52.75.Fk

I. INTRODUCTION

A vacuum thermionic energy conversion device (TEC) is a type of heat engine that converts heat directly to electrical work via the phenomenon of thermionic emission. A schematic and short description is shown in Fig. 1. Several theoretical descriptions of the operation of such devices have been derived using different assumptions.[1–4] A major problem affecting the performance of these devices has been the negative space charge effect. This effect is due to the electrons which are emitted into the evacuated interelectode space, causing a net buildup of negative charge. This negative space charge screens less energetic electrons from traversing the interelectrode space and contributing to the output current of the device. This limiting of the output current due to the negative space charge effect in turn limits the output power of the device, degrading the performance as an energy conversion device. The space charge effect can be substantial. One approach to mitigate the space charge effect is to reduce the interelectrode spacing to a few microns. However, such designs are difficult to engineer and fabricate. Despite the negative space charge effect, TEC's can efficiently convert heat to electrical work because there is no phononic transport across the active region of the device. Recent models of nanometer gap devices show that TEC's can achieve high efficiency at high output power for operating temperatures around 1000 K.[5]

Our approach to mitigating the negative space charge effect is not to reduce the interelectrode spacing, but to adjust the material properties of the emission surface: namely employ a hydrogen terminated diamond material which exhibits negative electron affinity. It has been shown that a hydrogen termination layer on (100), (110), (111), and polycrystalline diamond films results in a negative electron affinity (NEA) surface.[6–12] The negative electron affinity is a result of the dipole moment due to the hydrogen passivation layer which raises the conduction band minimum of the material above the vacuum level. Therefore any electron thermally promoted to the conduction band can potentially escape the emitter. Furthermore, the electrons that are thermionically emitted will have significant kinetic energy in contrast to a conventional material. Thus the NEA acts as a filter, preventing the slower electrons from being emitted, the electrons which are most responsible for the negative space charge effect, and most affected by space charge.

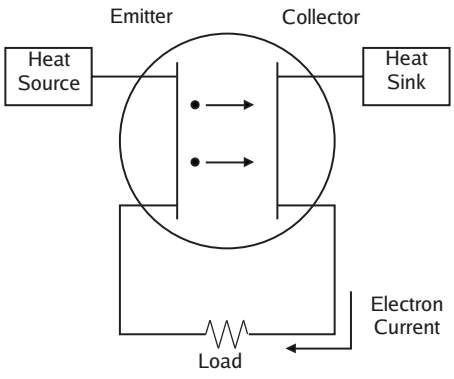

FIG. 1. Schematic diagram of a thermionic energy conversion device. In typical operation, the emitter is held at a higher temperature than the collector. Electrons are thermionically emitted from the emitter, travel across the interelectrode space, are collected by the collector, pass through the lead to the external load where work is done, then return to the emitter and complete the circuit.

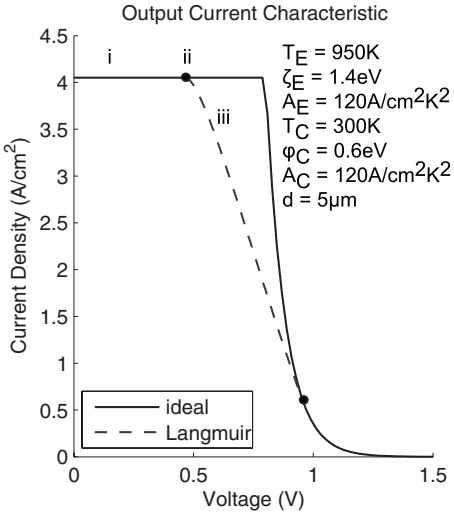

FIG. 2. Output current characteristics of the ideal and Langmuir models. Important points of the Langmuir model are labeled: (i) accelerating regime; (ii) saturation point; (iii) space charge limited regime.

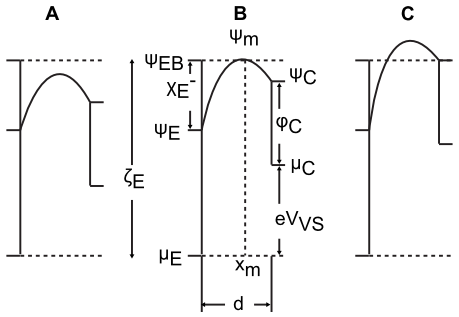

FIG. 3. Qualitative motive diagrams for a TEC device operating in the (A) accelerating regime, (B) at the virtual saturation point, and (C) in the space charge limited mode, respectively. The emitter and collector are separated by an evacuated space of distance d. The emitter conduction band minimum is denoted by ψ_{EB}, the vacuum level by ψ_E, and the Fermi energy by μ_E. The emitter barrier height and NEA are denoted by ζ_E and χ_E, respectively. The collector has a similar set of parameters including the work function (ϕ_C). The collector is held at an output voltage of eV and the maximum motive (ψ_m) occurs at the position x_m.

In this paper we develop a theory to calculate the virtual saturation point of the output current characteristic of a vacuum TEC with a NEA material as the emitter. The virtual saturation point is defined as the voltage such that the maximum motive occurs at the same height as the conduction band minimum of the emitter.

II. THEORETICAL BASICS

The regime of interest to this derivation is the so-called accelerating mode to the virtual saturation point. This region can be seen in Fig. 2 which depicts output current characteristic results from two TEC models featuring conventional (non-NEA) emitter materials: the ideal model[1] which ignores space charge, and the Langmuir model[1,2] which accounts for space charge. Both models ignore back emission because, for calculations performed in this study, the collector is at a sufficiently low temperature with respect to the emitter. In the figure, the accelerating mode is the branch of the curve labeled by "i," the virtual saturation point is labeled "ii," and the space charge limited mode is labeled "iii." The accelerating mode of the NEA device is the condition such that the maximum motive occurs at a level below the conduction band minimum. In this regime, all emitted electrons travel unimpeded across the interelectrode space and are collected. The output current in this case is given by the Richardson-Dushman equation $J_{ES}=AT_E^2\exp(-\zeta_E/kT_E)$, where J_{ES} indicates the emitter saturation current, A is the Richardson constant, T_E is the absolute emitter temperature, ζ_E is the emitter barrier height, and k is Boltzmann's constant.

A distinction between the meaning of work function and barrier height is in order. Work function is defined here as the energy difference between the vacuum level and Fermi energy of a material. In classical thermionics, the work function is the minimum energy required by an electron to be thermionically emitted, and space charge limited electron transport from such materials is given by Langmuir's model. For a positive electron affinity surface the work function represents the barrier to emission, while for an NEA surface the barrier height refers to the difference between the conduction band minimum and Fermi energy. In an NEA material, an electron promoted into the conduction band can potentially escape. Strictly speaking, the value of the NEA will determine the material's work function. However, in the case of thermionic emission from an NEA material, the barrier height, not the work function, is the metric of interest. When comparing the thermionic performance of a conventional positive electron affinity (PEA) material to that of an NEA material, the work function of the PEA material should be equal to the barrier height of the NEA material to obtain a fair comparison.

The space charge limited regime can be understood by considering a so-called motive diagram. Such motive diagrams and their descriptions for the case of a TEC with an NEA emitter are given in Fig. 3. The motive is related to the electrostatic potential by a factor of $-e$. As the output voltage at the collector is increased, the maximum motive increases up to the virtual saturation point which is the upper bound of voltage for the accelerating regime. For motives higher than the CBM, the current is space charge limited and the details of operation in this regime are not addressed here.

The objective of this study is to calculate the current and voltage at the virtual saturation point for a given set of device parameters. Determination of the virtual saturation point is fundamentally a self-consistency issue: the value of the output current affects the value of the output voltage of the collector. Due to this self-consistency issue, the output voltage is not *a priori* known; therefore simply appling boundary conditions to solve Poisson's equation is not an option. The strategy to calculate current and voltage at the virtual saturation point follows the same approach as developed in prior studies.[1,2] Briefly summarized: first, determine the electron distribution function, $f(x,v_e)$, in the interelectrode space.

Second, determine the electron number density $n_e(x)$. Third, cast Poisson's equation in a universal dimensionless form. Fourth, determine expressions for the output current J, the saturation current J_{ES}, and a relationship between the two. Finally, determine an algorithm based on the derived quantities to calculate the output current and voltage at the virtual saturation point. The collector temperature considered in this paper is sufficiently small with respect to the emitter temperature that back emission is negligible: in our case the emitter saturation current is roughly 5×10^3 greater than the collector saturation current.

A. Virtual saturation point

In the interelectrode space, the electrons are assumed to behave like a collisionless gas, and following Ref. 13, the distribution function of the electrons is given by Eq. (1):

$$f(x,v_e) = 2n_e(x_m)\left(\frac{m_e}{2\pi kT_E}\right)^{3/2}\exp\left(\frac{\psi_m-\psi}{kT_E}-\frac{m_e v_e^2}{2kT_E}\right)\times u\left[v_{ex}-\left(2\frac{\psi_m-\psi}{m_e}\right)^{1/2}\right]. \tag{1}$$

The following variables are used: $n_e(x_m)$, the number density of electrons at the point of maximum motive; m_e, electron mass; k, Boltzmann's constant; ψ_m, the maximum motive; ψ, the motive at point x; $v_e \equiv (v_{ex}^2+v_{ey}^2+v_{ez}^2)^{1/2}$, the magnitude of the velocity of the gas at a point in space; u, the unit step function.

In general, the number density of electrons $[n_e(x)]$ can be calculated from the distribution function by

$$n_e(x) = \int_{-\infty}^{\infty} dv_{ex}\int_{-\infty}^{\infty} dv_{ey}\int_{-\infty}^{\infty} dv_{ez} f(x,v_e). \tag{2}$$

In the case of the virtual saturation point, the electron number density is given by

$$n_e(x) = n_e(x_m)\exp\left(\frac{\psi_m-\psi}{kT_E}\right)\left\{1-\mathrm{erf}\left[\left(\frac{\psi_m-\psi}{kT_E}\right)^{1/2}\right]\right\}. \tag{3}$$

Poisson's equation can be cast in terms of the motive as opposed to the electrostatic potential as in

$$\frac{d^2\psi}{dx^2} = -\frac{e^2 n_e}{\epsilon_0}, \tag{4}$$

where ϵ_0 is the permittivity of free space.

The expression for the number density of electrons can be substituted into Poisson's equation, and through a change of variables the dimensionless Poisson's equation is given by

$$2\frac{d^2\gamma}{d\xi^2} = \exp(\gamma)[1-\mathrm{erf}(\gamma^{1/2})], \tag{5}$$

where $\gamma \equiv (\psi_m-\psi)/kT_E$, $\xi \equiv (x-x_m)/x_0$, $x_0^2 \equiv (\epsilon_0 kT_E)/[2e^2 n_e(x_m)]$, and the initial conditions are $\gamma(0)=0$ and $\gamma'(0)=0$. When $\xi>0$, this result is identical to the results of Langmuir.[13]

Before the virtual saturation voltage can be calculated, the output current density at the virtual saturation point must be calculated. In general, the output current density is given by the number of electrons passing the point of maximum motive and moving towards the collector:

$$J = e\int_0^{\infty} dv_{ex}\int_{-\infty}^{\infty} dv_{ey}\int_{-\infty}^{\infty} dv_{ez} v_{ex} f(x_m,v_e). \tag{6}$$

Evaluating the integrals, the output current density is then given by

$$J = 2en_e(x_m)\left(\frac{kT_E}{2\pi m_e}\right)^{1/2}. \tag{7}$$

Since the maximum motive and conduction band minimum are equal at the virtual saturation point, the emitter saturation current density (J_{ES}), which is given by the Richardson Dushman equation, is equal to the output current density given by Eq. (7).

The following procedure then can be used to calculate the virtual saturation point voltage.

(i) Calculate the solution to the dimensionless Poisson's equation given by Eq. (5).

(ii) Calculate the dimensionless motive just outside the emitter γ_E. According to Fig. 3(b), γ_E is given by

$$\gamma_E = \frac{\bar{\chi}_E}{kT_E}. \tag{8}$$

(iii) Use the solution to Eq. (5) to calculate the value of ξ_E corresponding to γ_E found in the previous step. The value ξ_E is the dimensionless distance just outside the emitter.

(iv) Calculate x_m from Eq. (9). This equation is derived from Eq. (7), the definitions of x_0 and ξ, and the fact that $J=J_{ES}$ at the virtual saturation point (if $x_m>d$, note the special case in the following subsection),

$$x_m = -\xi_E\left(\frac{\epsilon_0^2 k^3}{2\pi m_e e^2}\right)^{1/4}\frac{T_E^{3/4}}{J_{ES}^{1/2}}. \tag{9}$$

(v) Calculate the dimensionless distance just outside the collector ξ_C,

$$\xi_C = (d-x_m)\left(\frac{2\pi m_e e^2}{\epsilon_0^2 k^3}\right)^{1/4}\frac{J_{ES}^{1/2}}{T_E^{3/4}}. \tag{10}$$

(vi) Use the solution to Eq. (5) and the value of ξ_C to calculate the dimensionless motive just outside the collector γ_C.

(vii) According to Fig. 3(b) and the definition $\gamma_C = (\psi_m-\psi_C)/kT_E$ the virtual saturation point voltage V_{VS} can be calculated from

$$V_{VS} = \frac{-kT_E\gamma_C+\zeta_E-\phi_C}{e}. \tag{11}$$

B. Special case

A special case of this algorithm is when x_m from Eq. (9) is greater than the interelectrode spacing d. This special case

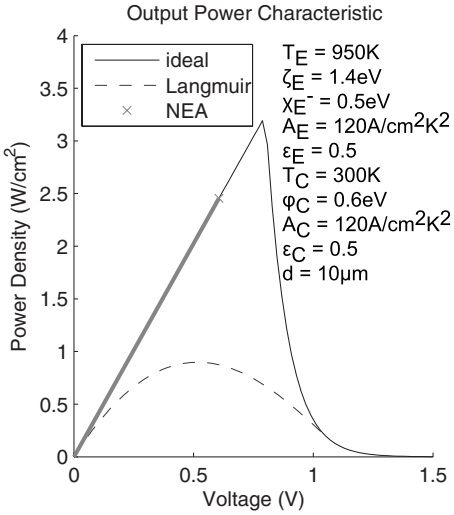

FIG. 4. Output power characteristics for the ideal (no space charge), Langmuir (space charge), and NEA models operating with the same set of parameters.

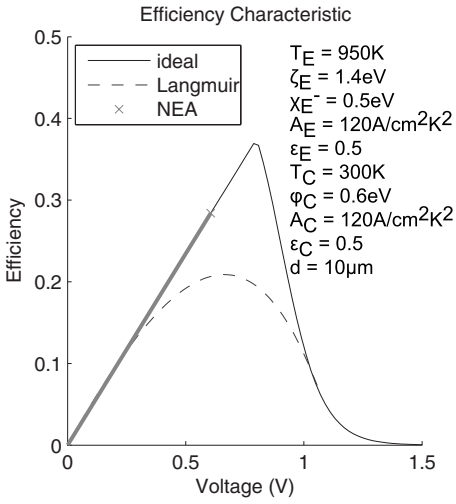

FIG. 5. Efficiency characteristics for the ideal, Langmuir, and NEA models operating with the same set of parameters.

can occur because neither the solution to the dimensionless Poisson equation given in Eq. (5), nor any of the quantities used in calculating x_m depend on the value of d. In this special case, the output voltage and output current density of the virtual saturation point is given by the contact potential $(\zeta_E - \phi_C)$ and the saturation current density, respectively. The motive can be determined by solving Poisson's equation given by Eq. (4) with the boundary conditions: $\psi(x=0) = \zeta_E - \chi_E^-$ and $\psi(x=d) = \zeta_E$.

III. IMPLEMENTATION, RESULTS, AND DISCUSSION

The algorithm described in the previous section was implemented as a computer program using MATLAB. Equation (5) is similar to Langmuir's dimensionless Poisson equation,[13] and therefore the relevant part of Kleynen's[14] tabulated solution was used. Cubic spline interpolation was used to determine intermediate points in the tabulation.

Nitrogen doped diamond was considered as an emitter material. According to temperature limited thermionic emission measurements[15] and ultraviolet photoemission spectroscopy measurements,[16] the barrier height of this material is around 1.4 eV. The diamond film was deposited on a molybdenum substrate using a plasma assisted chemical vapor deposition technique, with the plasma comprised of hydrogen and methane. The collector barrier height was taken to be 0.6 eV which may be achieved using a cesiated metal or diamond surface. The emitter was considered to be held at 950 K and the collector was held at 300 K. At a collector temperature of 300 K, the cesium should be stable and not desorb from the surface. Both emitter and collector Richardson's constants are assumed to be the theoretical value of 120 A/cm^2 K^2, and the interelectrode spacing is taken to be 10 μm. For the NEA emitter model, the value of the NEA is 0.5 eV. The value of the NEA was chosen conservatively despite higher reported values.[8,17]

In Fig. 4 the output power characteristics are shown for the three models. Each model was calculated using the same set of parameters shown in the caption in order to obtain a benchmark of how the NEA device performs. For the ideal model, the maximum output power is 3.19 W/cm^2 and occurs at a voltage of 0.8 V. For the Langmuir model, the maximum output power is 0.90 W/cm^2 and occurs at a voltage of 0.52 V. The virtual saturation point for the NEA device occurs at a voltage of 0.61 V, and the corresponding output power is 2.5 W/cm^2. Although the virtual saturation point of the NEA model is not necessarily the maximum output power of the device, this calculation establishes that the virtual saturation point power is significantly greater than the output power of the conventional device at the same output voltage. In general, a TEC with an NEA emitter should outperform a TEC with a conventional emitter in terms of output power.

Efficiency of these devices can be estimated by considering heat transport via the thermionic electrons $[Q_E = J(\psi_m - \mu_E + 2kT_E)/e]$ and Stefan-Boltzmann losses from the electrodes $[Q_r = \sigma_0(\epsilon_E T_E^4 - \epsilon_C T_C^4)]$, according to Hatsopoulous and Gyftopoulos[1] where ϵ_E and ϵ_C are the emissivities of the emitter and collector, respectively. The efficiency is given by

$$\eta = \frac{JV}{Q_E + Q_r}. \tag{12}$$

Efficiency characteristics are shown in Fig. 5, calculated using the same parameters as in Fig. 4 and additionally considering both emitter and collector electrodes to have emissivity of 0.5. At the virtual saturation point, the NEA model has an absolute efficiency of 28%. The ideal and Langmuir models have absolute efficiencies of 37% and 19%, respectively, at maximum power. The Carnot efficiency of a device operating between these temperatures is 68%.

In Fig. 6, the same set of parameters was used for the models, except that the interelectrode spacing of the Langmuir model was reduced until its saturation point was coincident with the virtual saturation point of the NEA model.

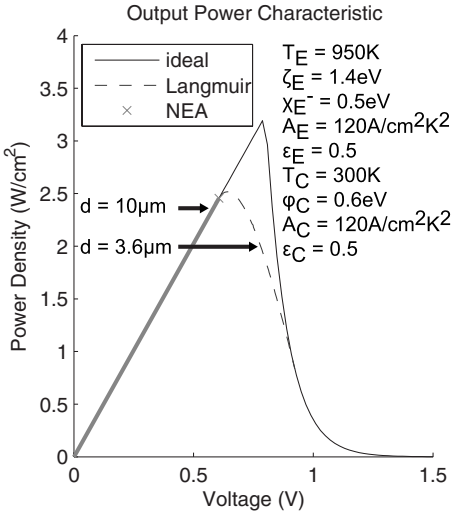

FIG. 6. Output power characteristics of the ideal, Langmuir, and NEA models. The NEA model is calculated at an interelectrode spacing of 10 μm, and the Langmuir model is calculated at an interelectrode spacing of 3.6 μm. At this distance, the saturation point of the Langmuir model coincides with the virtual saturation point of the NEA model.

The saturation point of the Langmuir model operating at $d=3.6$ μm is coincident with the virtual saturation point of the NEA model operating at $d=10$ μm. Our present computational capabilities of the NEA device do not allow a comparison of the maximum output power of the two devices, but the results establish that the NEA device can be designed with a significantly larger interelectrode spacing in order to perform at roughly the same output power as the device with conventional electrodes.

IV. CONCLUSIONS

The analysis presented here establishes that negative electron affinity emitters mitigate space charge and improve the performance of a vacuum TEC over a TEC with conventional electrodes. The NEA device generally has a higher output power and efficiency than the conventional device with similar operating parameters. Furthermore, the virtual saturation point of the NEA device occurs at a higher voltage than the corresponding saturation point of the conventional device, indicating that the space charge limited mode of the NEA device is smaller than that of the conventional device. Additionally, for devices which are operating at similar output power with similar operating parameters, the NEA device will have a larger interelectrode spacing which simplifies fabrication of the devices.

A more complete analysis which includes the entire space charge limited mode is necessary to completely characterize the performance of a TEC with an NEA emitter as well as to give a better comparison to a TEC with a conventional emitter material.

Experimental work is being performed concurrently in our lab to investigate the phenomenon of thermionic emission from nitrogen and phosphorus doped NEA diamond. At elevated temperatures, the hydrogen termination layer of a diamond surface will desorb, but the hydrogen termination layer on single crystal diamond should be stable at the temperatures discussed in this report. Investigations are underway in our lab to study this issue.

ACKNOWLEDGMENT

This research was supported by the Office of Naval Research through the TEC MURI program.

*jrsmith3@csu.edu

[1] G. N. Hatsopoulous and E. P. Gyftopoulos, *Thermionic Energy Conversion*, (MIT Press, Cambridge, MA, 1973), Vol. 1.
[2] G. N. Hatsopoulous and E. P. Gyftopoulos, *Thermionic Energy Conversion*, (MIT Press, Cambridge, MA, 1979), Vol. 2.
[3] Anthony F. Dugan, J. Appl. Phys. **31**, 1397 (1960).
[4] Joshua R. Smith, Robert J. Nemanich, and Griff L. Bilbro, Diamond Relat. Mater. **15**, 870 (2005).
[5] Y. C. Gerstenmaier and G. Wachutka, in *Proceedings of the 36th European Solid-State Device Research Conference*, 2006 (IEEE, Piscataway, NJ, 2007), pp. 431–434.
[6] F. J. Himpsel, J. A. Knapp, J. A. VanVechten, and D. E. Eastman, Phys. Rev. B **20**, 624 (1979).
[7] C. Bandis and B. B. Pate, Phys. Rev. B **52**, 12056 (1995).
[8] J. van der Weide, Z. Zhang, P. K. Baumann, M. G. Wensell, J. Bernholc, and R. J. Nemanich, Phys. Rev. B **50**, 5803 (1994).
[9] Eliane Schaller Léon Diederich, Olivier M. Küttel, and Louis Schlapbach, Surf. Sci. **349**, 176 (1996).
[10] P. K. Baumann and R. J. Nemanich, Surf. Sci. **409**, 320 (1998).
[11] P. Aebi L. Diederich, O. M. Küttel, and L. Schlapbach, Surf. Sci. **418**, 219 (1998).
[12] I. L. Krainsky, V. M. Asnin, G. T. Mearini, and J. A. Dayton, Phys. Rev. B **53**, R7650 (1996).
[13] Irving Langmuir, Phys. Rev. **21**, 419 (1923).
[14] P. H. J. A. Kleynen, Philips Res. Rep. **1**, 79 (1945).
[15] Franz A. M. Koeck and Robert J. Nemanich, Diamond Relat. Mater. **15**, 217 (2006).
[16] Y.-J. Tang, Ph.D. thesis, North Carolina State University, Raleigh, NC, 2007.
[17] J. B. Cui, J. Ristein, and L. Ley, Phys. Rev. Lett. **81**, 429 (1998).